Electron Transfer in Mixed-Valence Polyferrocenium Cations: Preparation, Electrochemistry, and ^{57}Fe Mössbauer Characteristics

Teng-Yuan Dong,*[,1] Wen-Yu Lee,[1] Pau-Tang Su,[1] Ling-Shao Chang,[1] and Kuan-Jiuh Lin[2]

Department of Chemistry, National Sun Yat-Sen University, Kaohsiung, Taiwan, and Institute of Chemistry, Academia Sinica, Nankang, Taipei, Taiwan

Received March 9, 1998

Convenient new methods are developed for the preparation of 1′,1‴″-disubstituted triferrocenes and tetraferrocenes that can be oxidized with iodine to a new series of mixed-valence compounds. The X-ray structures of 1′,1‴″-diethyltriferrocene, 1′,1‴″-dimethoxymethyltriferrocene, and 1′,1‴″-dimethoxymethyltetraferrocene have been determined at 298 K. The rates of intramolecular electron transfer in these mixed-valence cations were estimated by variable-temperature ^{57}Fe Mössbauer experiments. The features in all 80 and 300 K spectra include two doublets, one with a quadrupole splitting (ΔE_Q) of ∼2 mm s^{-1} (Fe(II) site) and the other with ΔE_Q = ∼0.3 mm s^{-1} (Fe(III) site). This pattern of two doublets is expected for a mixed-valence biferrocenium cation that is valence-trapped on the time scale of the Mössbauer technique (electron-transfer rate <∼10^7 s^{-1} in the solid state). The electrochemical measurements are also presented.

Introduction

The insight provided by the rich chemistry of bridged mixed-valence dimers, especially those of ruthenium dimers[3] and biferrocenium cations,[4] has promoted a great deal of both experimental and theoretical studies. Considerable work has been focused on the use of mixed-valence complexes to probe electron transfer between well-separated metal sites. In the case of mixed-valence biferrocenium cations (fulvalenide-bridged compounds), it has been studied extensively in the solid state regarding the nature of the structural factors and lattice dynamics.[5] Despite considerable work in biferrocenium cations, however, the mixed-valence chemistry of ferrocenium oligomers larger than biferrocenium is virtually unknown.[6,7] This paper is concerned with the oxidation products of triferrocenes and tetraferrocenes (Chart 1, **1**−**7**).

Few mixed-valence ferrocenyl compounds that have been prepared up to this time contain more than two ferrocenyl units. Tetraferrocenylporphyrin^{3+}(I_3^-)$_3$, **8**, has been well characterized to be localized on the ^{57}Fe Mössbauer time scale (electron-transfer rate < 10^7 s^{-1}).[8] Furthermore, upon lowing the temperature to 90 K, the Mössbauer spectra of **8** show that the ferrocene-to-ferrocenium ratio increases, as indicated by fitting the areas of the Fe^{II} and Fe^{III} doublets. A migration of electron density from the porphyrin ring at low temperatures was proposed.

Chart 1

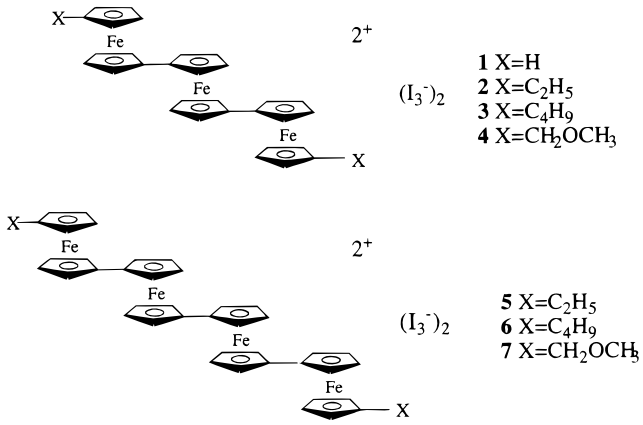

The first single-crystal X-ray structure of the mixed-valence ferrocenium(III)−trisferrocenyl(II) borate, **9**, was communicated.[9] The centroid-to-centroid distance between the two cyclopentadienyl (Cp) rings in one ferrocenyl moiety was found to be longer than the corresponding distance in the other three metallocene units. Unfortunately, no ^{57}Fe Mössbauer, EPR, or spectroscopic data other than electronic absorption data have been reported as yet for this compound.

In 1974, Meyer and co-workers reported the electrochemical generation of the mixed-valence ions of poly-

(1) National Sun Yat-Sen University.
(2) Academia Sinica.
(3) For reviews, see: (a) Day, P. *Int. Rev. Phys. Chem.* **1981**, *1*, 149. (b) *Mixed-Valence Compounds, Theory and Applications in Chemistry, Physics, Geology and Biology*; Brown, D. B., Ed.; Reidel Publishing Co.: Boston, MA, 1980. (c) Creutz, C. *Prog. Inorg. Chem.* **1983**, *30*, 1−73. (d) Richardson, D. E.; Taube, H. *Coord. Chem. Rev.* **1984**, *60*, 107.
(4) Dong, T.-Y.; Lee, S. H.; Chang, C. K.; Lin, H. M.; Lin, K. J. *Organometallics* **1997**, *16*, 2773 and references therein.
(5) Dong, T.-Y.; Chang, C. K.; Lee, S. H.; Lai, L. L.; Chiang, M. Y. N.; Lin, K. J. *Organometallics* **1997**, *16*, 5816 and references therein.
(6) Cowan, D. O.; Kaufman, F. *J. Am. Chem. Soc.* **1970**, *92*, 219.
(7) Brown, G. M.; Meyer, T. J.; Cowan, D. O.; LeVanda, C.; Kaufman, F.; Roling, R. V.; Raush, M. D. *Inorg. Chem.* **1975**, *14*, 506.
(8) Wollmann, R. G.; Hendrickson, D. N. *Inorg. Chem.* **1977**, *16*, 3079.
(9) Cowan, D. O.; Shu, P.; Hedberg, F. L.; Rossi, M.; Kitsenmacher, T. J. *J. Am. Chem. Soc.* **1979**, *101*, 1304.

S0276-7333(98)00170-8 CCC: $15.00
Publication on Web 06/26/1998

Chart 2

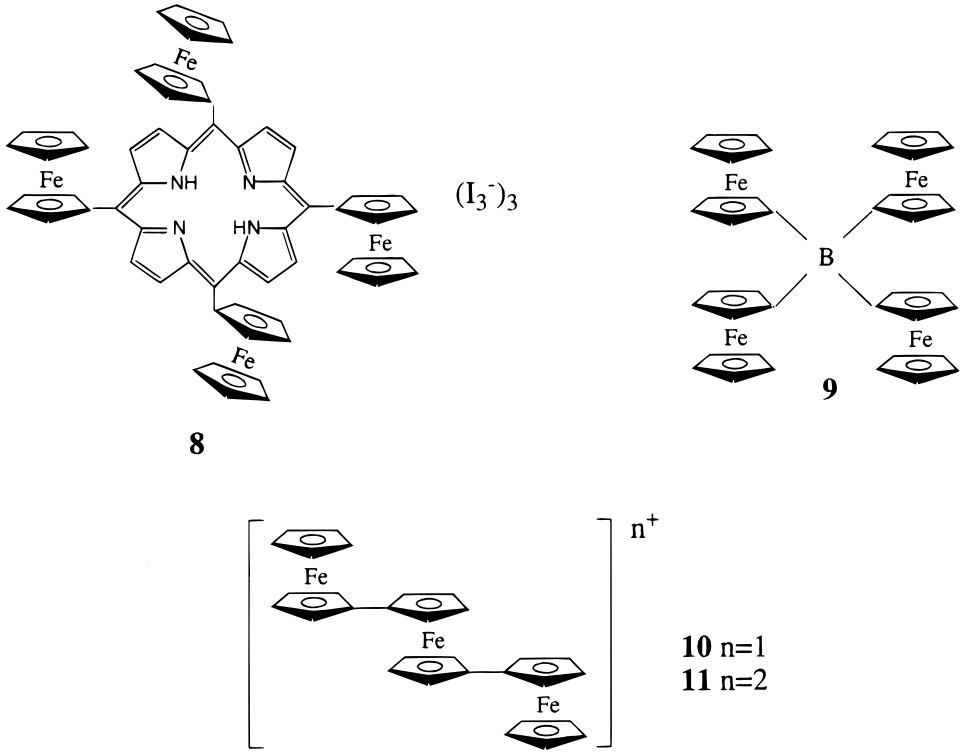

Chart 3

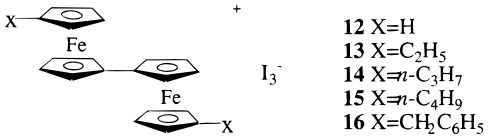

ferrocenes (**10** and **11**).[7] They found that a series of one-electron waves is observed by cyclic voltammetry, corresponding to one wave per ferrocenyl unit. The electrochemically generated mixed-valence monocation **10** (Chart 2) has an intervalence transfer electronic absorption band at 1990 nm ($\epsilon = 1560$ cm^{-1} M^{-1}). In the case of dication **11**, an intervalence transfer band is observed at 1670 nm ($\epsilon = 1080$ cm^{-1} M^{-1}).

The present study began with efforts to prepare the neutral disubstituted triferrocenes and tetraferrocenes, selectively oxidize the iron centers, and then study the electronic properties which may be compared to those of other mixed-valence ferrocenyl cations.

Results and Discussion

In the solid state, it has been demonstrated that relatively minor perturbations caused by the substituents on the Cp ring in mixed-valence biferrocenium cations have dramatic effects on the electronic structure and rate of intramolecular electron transfer.[4] Estimated by ^{57}Fe Mössbauer techniques, the mixed-valence cation **12** (Chart 3) has a valence-trapped electronic structure at 300 K (rate $< 10^7$ s^{-1}). However, the mixed-valence dialkylbiferrocenium cations **13**−**16** give unusual temperature-dependent Mössbauer spectra.[10] The Mössbauer results indicate that cations **13**−**16** are valence-detrapped (rate $> 10^7$ s^{-1}) at temperatures above 275, 245, 275, and 260 K, respectively.[11−15] Thus, we undertook the present work in the hope that a similar phenomenon could also be observed for the valence-trapped triferrocenium dication **1** reported before. In addition to the studies of electron transfer, the series of triferrocenes and tetraferrocenes can also provide rather versatile electrochemical and magnetic chemistry.

Dialkyltriferrocenes and dialkyltetraferrocenes were prepared by coupling the corresponding bromoferrocenes, using activated Cu as the catalyst (Schemes 1 and 2). Mixed-valence compounds were prepared by oxidizing the neutral triferrocenes and tetraferrocenes with I_2. Before the new physical data are described, a summary of the single-crystal X-ray structural results obtained for **23**, **25**, and **29** will be presented.

Molecular Structures of Triferrocenes 23 and 25. The results of our crystallographic studies at room temperature show that **23** and **25** crystallize in the monoclinic space group $P2_1/c$ and monoclinic space group $P2_1/n$, respectively. Details of the X-ray crystal data collections and unit cell parameters are given in Table 1. ORTEP drawings of the molecules are shown in Figure 1, and bond distances and angles are given as Supporting Information. An interesting finding is that the two ethyl substituents on the Cp rings in **23** are situated differently, and this is in contrast to compound **25** in which the $-CH_2OCH_3$ groups positioned

(10) Dong, T.-Y.; Hendrickson, D. N.; Iwai, K.; Cohn, M. J.; Rheingold, A. L.; Sano, H.; Motoyama, S. *J. Am. Chem. Soc.* **1985**, *107*, 7996.
(11) Hendrickson, D. N.; Oh, S. M.; Dong, T.-Y.; Moore, M. F. *Comm. Inorg. Chem.* **1985**, *4*, 329.
(12) Dong, T.-Y.; Cohn, M. J.; Hendrickson, D. N.; Pierpont, C. G. *J. Am. Chem. Soc.* **1985**, *107*, 4777.
(13) Cohn, M. J.; Dong, T.-Y.; Hendrickson, D. N.; Geib, S. J.; Rheingold, A. L. *J. Chem. Soc., Chem. Commun.* **1985**, 1095.
(14) Dong, T.-Y.; Hendrickson, D. N.; Iwai, K.; Cohn, M. J.; Rheingold, A. L.; Sano, H.; Motoyama, S. *J. Am. Chem. Soc.* **1985**, *107*, 7996.
(15) Iijima, S.; Saida, R.; Motoyama, I.; Sano, H. *Bull. Chem. Soc. Jpn.* **1981**, *54*, 1375.

Scheme 1[a]

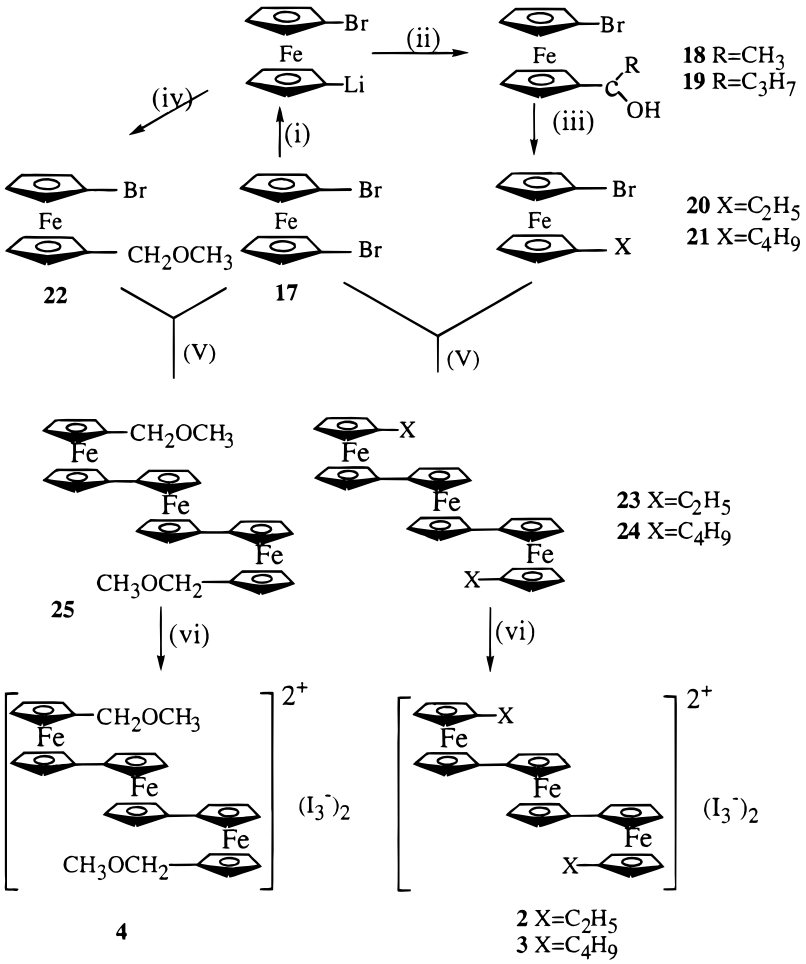

[a] (i) 1.0 eq *n*-BuLi. (ii) RCHO. (iii) $LiAlH_4/AlCl_3$. (iv) ICH_2OCH_3. (v) Cu. (vi) 3 equiv of I_2.

above and below the central ferrocenyl moiety are crystallographically equivalent. Consequently, the molecular structure of **23** is different from **25**. In the case of **25**, the molecular structure can be described as steplike ferrocenyl moieties. This usual type of steplike conformation has been seen in other triferrocenyl compounds. As shown in Figure 1, the molecular structure of **23** can be described as column of ferrocenyl moieties. Furthermore, there is a Cp−Cp $\pi-\pi$ interaction (~3.3 Å) between the two terminal ferrocenyl units.

As given in Table 2, a direct comparison of the average Fe−C and Fe−Cp ring distances is made. Inspection of the average bond distance between the Fe atom and the five carbons (Fe−C) of a given Cp ring and the average Fe−Cp distance for a ferrocenyl moiety indicates that these values are closer to the corresponding value observed for ferrocene (2.045 Å for Fe−C, 1.65 Å for Fe−Cp)[16] than the corresponding value observed for ferrocenium cation (2.075 Å for Fe−C, 1.70 Å for Fe−Cp).[17] The C−C bond length in the Cp rings in these compounds also agrees well with that in ferrocene (1.42 Å).[16] As shown in Table 2 (ta (dihedral angle between the two Cp rings associated with the corresponding Fe atom) values), the two least-squares planes of the Cp rings for a given ferrocenyl moiety in **23** and **25** form a nearly parallel geometry. Furthermore, the two Cp rings for a given ferrocenyl moiety are nearly eclipsed (see the sa (stagger angle between the two Cp rings associated with the corresponding Fe atom) values in Table 2), except the central ferrocenyl moiety in **25**. In **25**, the two Cp rings associated with Fe1 form a perfectly staggered conformation.

Molecular Structures of Tetraferrocene 29. Compound **29** crystallizes in the triclinic space group $P\bar{1}$. Figure 2 shows the molecular structure and atomic-labeling scheme. The site symmetry imposed on the molecule obviously requires that the two $-CH_2OCH_3$ substituents are in equivalent positions; this is similar to compound **25**. However, the structural conformation of **29** is different from **25**. As mentioned before, the molecular structure of **25** can be described as steplike ferrocenyl moieties. In the case of **29**, it can be described as column of ferrocenyl moieties, similar to compound **23**. Similarly, there is a Cp−Cp $\pi-\pi$ interaction (~3.3 Å) between the Fe1 and Fe2 ferrocenyl moieties. As shown in Table 2, the two Cp rings for a given ferrocenyl moiety form a nearly parallel geometry and eclipsed conformation.

Electrochemical Measurements. Electrochemical data for the neutral compounds **23**−**25** and **27**−**29**, as well as those for some other relevant compounds, are shown in Table 3. For all of the compounds studied, the number of waves observed by cyclic voltammetry

(16) Seiler, P.; Dunitz, J. D. *Acta Crystallogr., Sect. B* **1979**, *35*, 1068.
(17) Mammano, N. J.; Zalkin, A.; Landers, A.; Rheingold, A. L. *Inorg. Chem.* **1977**, *16*, 297.

Scheme 2

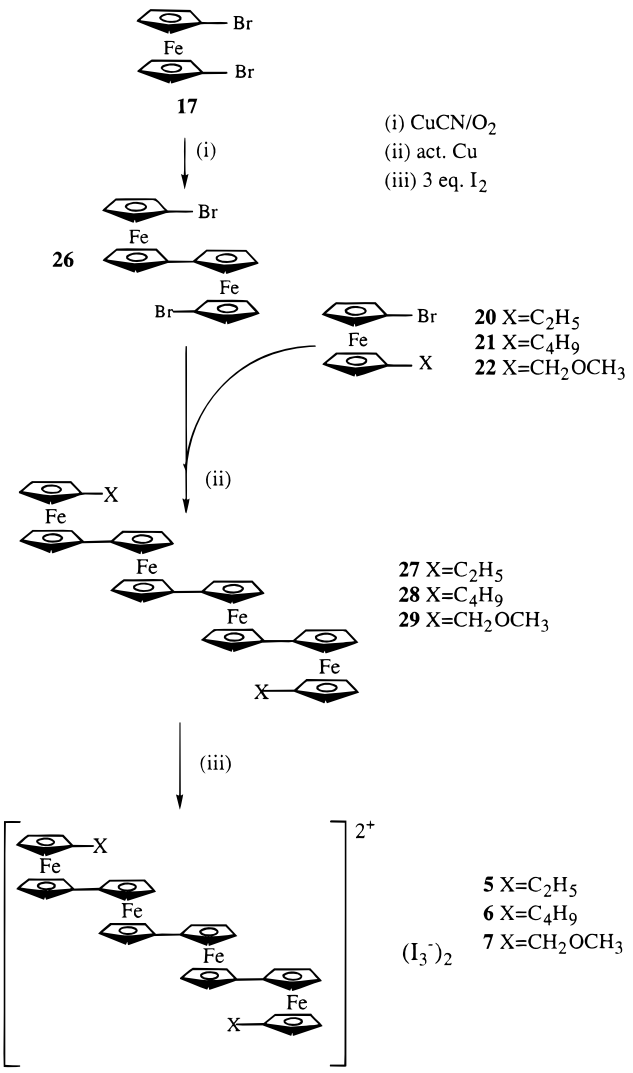

Table 1. Experimental and Crystal Data for the X-ray Structures

	23	**25**	**29**
formula	$C_{34}H_{34}Fe_3$	$C_{34}H_{34}Fe_3O_2$	$C_{44}H_{42}Fe_4O_2$
mol wt	610.18	642.18	826.20
cryst syst	monoclinic	monoclinic	triclinic
space group	$P2_1/c$	$P2_1/n$	$P\bar{1}$
a, Å	14.498(5)	13.738(1)	5.937(2)
b, Å	7.680(5)	7.503(1)	9.4772(7)
c, Å	23.62(2)	14.764(2)	17.874(2)
α, deg			92.424(9)
β, deg	94.29(5)	116.888(9)	97.76(2)
γ, deg			105.91(2)
ρ_{calcd}, gcm^{-3}	1.546	1.571	1.609
V, Å^3	2622(3)	1357.2(3)	955.0(4)
Z	4	2	1
μ, mm^{-1}	1.66	1.61	1.67
λ, Å	0.70930	0.70930	0.70930
2θ limits, deg	49.8	54.8	50.0
R_f[a]	0.090	0.033	0.030
R_{wf}[b]	0.105	0.038	0.034

[a] $R_f = \Sigma(||F_o| - |F_c||)/\Sigma|F_o|$. [b] $R_{wf} = \Sigma[(w(F_o - F_c)^2)/\Sigma(wF_o^2)]^{1/2}$.

(CV) was equal to the number of ferrocenyl groups. Electrochemical reversibility is demonstrated by the peak-to-peak separation (Δ in Table 3) between the resolved reduction and oxidation wave maxima. In fact, Δ is larger than the theoretical value of 59 mV. Under our experimental conditions, the ferrocene−ferrocenium couple has Δ = 70 mV, which is used as the criterion for reversibility. From CV, triferrocenes (**23**−**25**) undergo three electrochemically reversible one-electron oxidations. In the case of tetraferrocenes (**27**−**29**), they undergo four electrochemically reversible one-electron oxidations.

The effect of the substituents on the stability of the Fe(III) state is illustrated by the shift of the half-wave potential. In general, electron-donating groups stabilize the ferrocenium cation, lowering the half-wave potential, while electron-withdrawing groups have the opposite effect. Substituent effects on $E_{1/2}$ have been shown to be additive by potential measurements.[7]

For compounds **23**−**29**, there are chemically different sites (X−Fc and −Fc−) in the polymeric units. Upon oxidation to the mixed-valence ions, more than one oxidation state can exist. Consequently, the isomers may differ in free energy. For example, the dication of triferrocenes can exist as one of two energetically equivalent isomers, X−Fc$^+$−Fc$^+$−Fc−X and X−Fc−Fc$^+$−Fc$^+$−X, or as the energetically nonequivalent isomer X−Fc$^+$−Fc−Fc$^+$−X (Figure 3). Of course, the distribution between the various isomers will depend on the zero-point energy difference(s) (E_o) between them. It has been shown that estimation of the zero-point energy difference between isomers is possible. For example, it is possible to estimate the E_o value between the isomers C_2H_5−Fc$^+$−Fc$^+$−Fc−C_2H_5 and C_2H_5−Fc$^+$−Fc−Fc$^+$−C_2H_5. From the $E_{1/2}$ values in Table 3, ethylferrocene and 1′,1‴-diethylbiferrocene are more easily oxidized than ferrocene. Therefore, the substituent effects of the ethyl group and ethylferrocenyl group can be calculated.

$$\delta_{-C_2H_5} = E_{1/2}(C_2H_5Fc^{+,0}) - E_{1/2}(Fc^{+,0}) = -0.05\ \text{V}$$

$$\delta_{-C_2H_5Fc} = E_{1/2}((C_2H_5{-}Fc)_2^{+,0}) - E_{1/2}(Fc^{+,0}) - \delta_{-C_2H_5}$$

$$= 0.26 - 0.4 - (-0.05) = -0.09\ \text{V}$$

The potential for the reaction $C_2H_5Fc^+$−Fc$^+$−Fc−C_2H_5 + e → C_2H_5−Fc$^+$−Fc−Fc−C_2H_5 can be calculated.

$$E_{1/2}(\text{calcd}) = E_{1/2}(C_2H_5{-}Fc_2^{2+,+}) + \delta(C_2H_5{-}Fc) = 0.64 - 0.09 = 0.55\ \text{V}$$

Since $E_{1/2}$ (0.35 V) for the couple (C_2H_5−Fc−Fc−Fc−C_2H_5)$^{2+,+}$ is significantly lower, the experimental value must refer, mainly, to the reaction

$$C_2H_5{-}Fc^+{-}Fc{-}Fc^+{-}C_2H_5 + e \rightarrow C_2H_5{-}Fc{-}Fc^+{-}Fc{-}C_2H_5\ (E = 0.35\ \text{V})$$

By combining the half-reactions, the zero-point energy difference between the isomers C_2H_5−Fc$^+$−Fc−Fc$^+$−C_2H_5 and C_2H_5−Fc$^+$−Fc$^+$−Fc−C_2H_5 is estimated to be 0.2 V which is significantly larger than the E_o value (0.12 V) between the isomers Fc$^+$−Fc−Fc$^+$ and Fc$^+$−Fc$^+$−Fc.[7] We believe that this difference of the E_o values is a result of the electronic effect of the ethyl substituent. The nature of the substituent has a direct influence on the magnitude of E_o. As shown in Figure

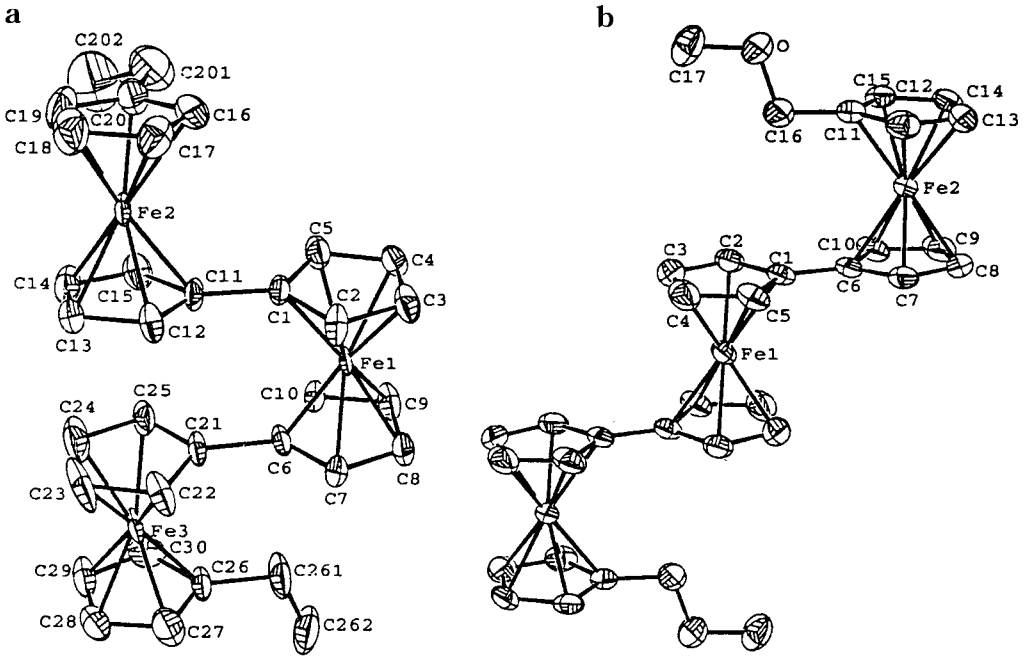

Figure 1. (a) ORTEP drawings for **23** and (b) **25**.

Table 2. Comparison of Atomic Distances (Å) and Angles (deg)

	23	**25**	**29**
Fe1−C[a]	2.04(1)	2.048(3)	2.053(3)
Fe2−C[a]	2.04(1)	2.040(3)	2.051(4)
Fe3−C[a]	2.04(1)		
Fe1−Cp[b]	1.651(6)	1.652(2)	1.660(2)
Fe2−Cp[b]	1.656(6)	1.648(2)	1.652(2)
Fe3−Cp[b]	1.656(6)		
ta (Fe1)[c]	1.9(5)	0.0	1.7(2)
ta (Fe2)[c]	1.6(5)	3.7(2)	1.9(2)
ta (Fe3)[c]	1.9(6)		
sa (Fe1)[d]	2.0(7)	36.0(1)	1.5(2)
sa (Fe2)[d]	2.9(8)	4.6(2)	1.0(2)
sa (Fe3)[d]	3.6(8)		

[a] Average Fe−C distance. [b] The distance between the Fe atom and the Cp ring. [c] The dihedral angle between the two Cp rings associated with the corresponding Fe atom. [d] Stagger angle between the two Cp rings associated with the corresponding Fe atom.

3, an electron-donating substituent can exert somewhat more influence on the X−Fc^+−Fc−Fc^+−X energy surface than on the X−Fc^+−Fc^+−Fc−X energy surface. It is important to realize that energetically it is the X−Fc^+−Fc−Fc^+−X energy surface in Figure 3 which is stabilized more by an electron-releasing substituent. With respect to the X−Fc^+−Fc−Fc^+−X energy surface, the stabilization in X−Fc^+−Fc^+−Fc−X energy surface by an electron-releasing substituent will be smaller. The net result shows an increase of the E_o value in a triferrocenium dication with an electron-donating substitutent. As shown in Table 3, the disproportionation constants K_c can be calculated from the values of $\Delta E_{1/2}$.

^{57}Fe Mössbauer Characteristics. The rates of intramolecular electron transfer in the mixed-valence cations **2**−**7** were estimated by ^{57}Fe Mössbauer spectroscopy (time scale $\sim 10^7$ s^{-1}). The various absorption peaks were fitted to Lorentzian lines. The resulting parameters are collected in Table 4. All of the ^{57}Fe Mössbauer spectra for mixed-valence compounds **2**−**7** show two doublets (Fe(II), $\Delta E_Q = 2.0$ mm s^{-1}; Fe(III), $\Delta E_Q = 0.3$ mm s^{-1}), which is characteristic of a valence-trapped cation in which the rate of intramolecular electron transfer is less than $\sim 10^7$ s^{-1}. For **2**−**4**, the ferrocene-to-ferrocenium area ratio is fitted into 1:2. The 1:2 ferrocene-to-ferrocenium relative area is expected for **2**−**4** if two of the ferrocenyl groups are oxidized. In the case of **5** and **6**, the ferrocene-to-ferrocenium area ratio is fitted into 2:2. The 2:2 ferrocene-to-ferrocenium area ratio for **5** and **6** indicates that two of the ferrocenyl groups are oxidized. An interesting observation in the cations of **5** and **7** is that ΔE_Q values for ferrocenium centers are much larger than those observed for triferrocenium cations. The larger ΔE_Q in the cations of **5** and **7** can be interpreted by assuming that the increased amount of overlap between the $^2E_{2g}$ and $^1A_{1g}$ states of

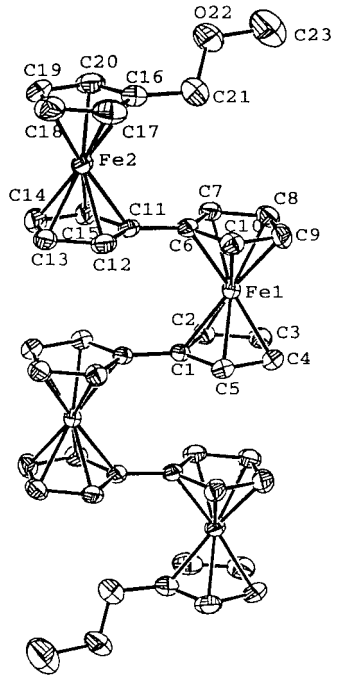

Figure 2. ORTEP drawing for **29**.

Table 3. Cyclic Voltammetry for Various Biferrocenes

compd	$E_{1/2}$,[a] V	$\Delta E_{1/2}$,[b] V	Δ,[c] mV	K_c ($\times 10^{-5}$)
ferrocene	0.40		70	
ethylferrocene	0.35		65	
methoxymethylferrocene	0.41		79	
biferrocene	0.31	0.32	70	2.65
	0.63		75	
1′-ethylbiferrocene	0.28	0.36	70	12.6
	0.64		85	
1′,1‴-diethylbiferrocene	0.26	0.33	65	3.92
	0.59		65	
1′-butylbiferrocene	0.28	0.37	75	18.7
	0.65		72	
1′,1‴-dibutylbiferrocene	0.26	0.32	65	2.65
	0.58		65	
1′,1‴-dimethoxymethyl-biferrocene	0.40	0.32	70	2.65
	0.72		72	
triferrocene	0.22	0.22		0.0536
	0.44	0.38		27.6
	0.82			
tetraferrocene	0.16	0.2		0.0245
	0.36	0.25		0.173
	0.61	0.28		0.057
	0.89			
23	0.19	0.16	68	0.00515
	0.35	0.45	73	424
	0.80		68	
24	0.19	0.16	71	0.00515
	0.35	0.45	66	424
	0.80		65	
25	0.25	0.20	72	0.0245
	0.45	0.35	69	8.55
	0.80		61	
27	0.19	0.12	65	0.00108
	0.31	0.27	65	0.377
	0.58	0.28	68	0.557
	0.86		70	
28	0.20	0.12	57	0.00108
	0.32	0.28	55	0.557
	0.60	0.27	62	0.377
	0.87		90	
29	0.20	0.18	64	0.00112
	0.38	0.22	67	0.0536
	0.60	0.23	57	0.0790
	0.83		87	

[a] All half-wave potentials are referred to the SCE electrode. [b] Peak separation between waves. [c] Peak-to-peak separation between the resolved reduction and oxidation wave maxima.

the ferrocenium and ferrocene portions of the molecular results in increased electron density at the ferrocenium centers.

Influence of Zero-Point Energy Difference on Electron Transfer. The goal of this section is to present an explanation for the differences of electron-transfer rates between biferrocenium cations **12**−**16** and polyferrocenium cations **1**−**7**.

Recently, there has been considerable progress made in understanding what factors control the rate of intramolecular electron transfer in the solid state for mixed-valence biferrocenium salts.[10−12,14,15] Hendrickson suggested that what is affecting the Mössbauer spectrum and impacting the temperature dependence is the onset of lattice dynamics (a second-order phase transition). In Hendrickson's theoretical model,[18] the factors that are potentially important in controlling the rate of intramolecular electron transfer in a mixed-valence biferrocenium cation include the effective barrier for

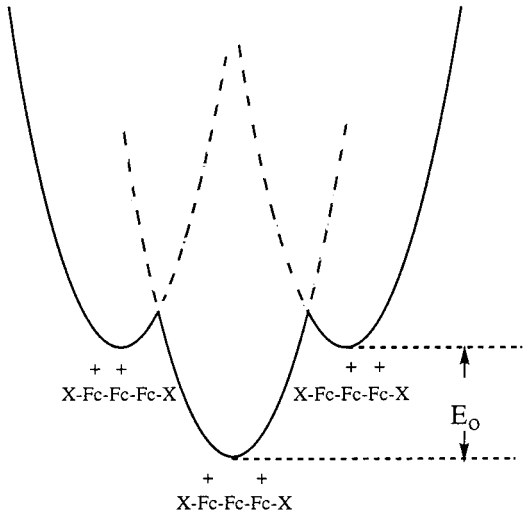

X: electron-donating groups

Figure 3. Potential energy-configurational diagrams for dication triferrocenium ions.

Table 4. ^{57}Fe Mössbauer Least-Squares-Fitting Parameters

compd	T, K	ΔE_Q[a]	δ[b]	Γ[c]
1	300	1.970	0.472	0.264; 0.256
		0.371	0.453	0.416; 0.390
2	300	2.045	0.328	0.169; 0.159
		0.209	0.297	0.360; 0.360
	80	2.073	0.425	0.154; 0.147
		0.329	0.418	0.245; 0.278
3	300	2.006	0.337	0.215; 0.199
		0.299	0.257	0.332; 0.332
	80	2.074	0.423	0.148; 0.142
		0.374	0.414	0.210; 0.239
4	300	2.047	0.344	0.140; 0.147
		0.235	0.335	0.359; 0.359
	80	2.050	0.426	0.139; 0.150
		0.235	0.424	0.255; 0.271
5	300	1.882	0.337	0.187; 0.238
		0.501	0.307	0.371; 0.403
6	300	1.954	0.328	0.251; 0.251
		0.349	0.265	0.402; 0.402
7	300	1.742	0.441	0.409; 0.378
		0.651	0.417	0.744; 0.545

[a] Quadrupole-splitting in mm s^{-1}. [b] Isomer shift referenced to iron-foil in mm s^{-1}. [c] Full-width at half-height taken from the least-squares-fitting program. The width for the line at more positive velocity is listed first for each doublet.

charge oscillation in the anion and the intermolecular cation−cation and cation−anion interactions. In our primary paper,[19] we found that there is a significant influence in the electron-transfer rate in the mixed-valence biferrocenium salt when the cyclopentadienyl (Cp) rings in each ferrocenyl moiety are tilted from the parallel geometry. Deviations of the Cp rings from the parallel position were found to correlate quite well with the critical temperature (T_c) of electronic delocalization−localization in biferrocenium salts. In a qualitative view, we suggest that there is an increased ($d_{x^2-y^2}$, d_{xy})-ring overlap as the tilt angle increases.

In fact, we believe that the most important factor in controlling the intramolecular electron transfer is the symmetry of the cation. For an asymmetric biferrocenium cation, the two irons are not in equivalent en-

(18) Kambara, T.; Hendrickson, D. N.; Dong, T.-Y.; Cohn, M. J. *J. Chem. Phys.* **1987**, *86*, 2362.

(19) Dong, T.-Y.; Huang, C. H.; Chang, C. K.; Wen, Y. S.; Lee, S. L.; Chen, J. A.; Yeh, W. Y.; Yeh, A. *J. Am. Chem. Soc.* **1993**, *115*, 6357.

Table 5. Physical Properties of Various Ferrocenes

compd	^{1}H NMR ($CDCl_3$, ppm)	MS (M^+ at *m/z*)	mp
18	1.45 (d, 3H, $-CH_3$), 2.01 (d, 1H, $-OH$), 4.12 (t, 2H, Cp), 4.22 (m, 4H, Cp), 4.42 (m, 2H, Cp), 4.66 (m, 1H, $-CH$)	308, 310	
19	0.93 (t, 3H, $-CH_3$), 1.46 (m, 2H, $-CH_2-$), 1.64 (m, 2H, $-CH_2-$), 2.06 (s, 1H, $-OH$), 4.13 (s, 2H, Cp), 4.22 (m, 4H, Cp), 4.42 (m, 3H, Cp, $-CH$)	336, 338	
23	1.02 (t, 6H, $-CH_3$), 2.11 (q, 4H, $-CH_2-$), 3.81 (d, 4H, Cp), 3.83 (d, 4H, Cp), 4.02 (t, 4H, Cp), 4.07 (t, 4H, Cp), 4.10 (t, 4H, Cp), 4.16 (t, 4H, Cp)	610	102−103
24	0.84 (t, 6H, $-CH_3$), 1.26 (m, 8H, $-CH_2-$), 2.06 (t, 6H, $-CH_2-$), 3.80 (d, 4H, Cp), 3.83 (t, 4H, Cp), 4.02 (t, 4H, Cp), 4.07 (t, 4H, Cp), 4.09 (t, 4H, Cp), 4.15 (t, 4H, Cp)	666	100−101
25	3.18 (s, 6H, $-OCH_3$), 3.91 (s, 4H, $-CH_2-$), 3.95 (d, 8H, Cp), 4.04 (d, 8H, Cp), 4.11 (s, 4H, Cp), 4.17 (s, 4H, Cp)	642	136−137
27	1.00 (t, 6H, $-CH_3$), 2.09 (q, 4H, $-CH_2-$), 3.79 (s, 4H, Cp), 3.80 (s, 4H, Cp), 3.98 (s, 12H, Cp), 4.03 (s, 4H, Cp), 4.07 (s, 4H, Cp), 4.11 (s, 4H, Cp)	794	110−112
28	0.82 (t, 6H, $-CH_3$), 1.25 (m, 8H, $-CH_2CH_2-$), 2.03 (t, 4H, $-CH_2-$), 3.77 (s, 4H, Cp), 3.79 (s, 4H, Cp), 3.97 (s, 12H, Cp), 4.01 (s, 4H, Cp), 4.04 (s, 4H, Cp), 4.09 (s, 4H, Cp)	850	162−163
29	3.17 9s, 6H, $-OCH_3$), 3.89 (s, 4H, $-CH_2-$), 3.92 (s, 4H, Cp), 3.94 (s, 8H, Cp), 3.97 (s, 4H, Cp), 3.98 (s, 4H, Cp), 4.01 (s, 4H, Cp), 4.08 (s, 4H, Cp), 4.13 (s, 4H, Cp)	826	157−158

vironments and this asymmetry results in a zero-point energy difference for intramolecular electron transfer. In other words, one vibronic state of the mixed-valence cation is energeically more stable than the other state. This explains why a delocalized electronic structure for an asymmetic biferrocenium cation has not been observed.

As mentioned in the Introduction, the symmetric mixed-valence compounds **13**−**16** have a delocalized electronic structure at 300 K. However, the 300 K Mössbauer spectra of **2**−**7** indicate the presence of a localized electronic structure. Here, we suggest that the most important factor in controlling the electron transfer in **2**−**7** is the presence of the zero-point energy difference (E_o). As shown in Figure 3, the electron-transfer products in mixed-valence cations **2**−**7** are energetically unfavorable oxidation-state isomers. For example, there are actually two equivalent unfavorable oxidation-state isomers for mixed-valence triferrocenium dications. Thus, one vibronic state of the mixed-valence dication is energetically more stable than the other state. This explains why a localized electronic structure for **2**−**7** was observed.

Experimental Section

General Information. All manipulations involving air-sensitive materials were carried out using standard Schlenk techniques under an atmosphere of N_2. Chromatography was performed on neutral alumina (Merck, activity II). Solvents were dried as follows: benzene, hexane, ether, and THF distilled from Na/benzophenone; CH_2Cl_2 and $(CH_3)_2S_2$ distilled from CaH_2. Samples of 1,1′-dibromoferrocene, **22**, and **26** were prepared according to the literature procedure.[5,20]

Syntheses of 18 and 19. Dibromoferrocene (**17**, 8.88 g, 20 mmol) was placed in a freshly oven-dried three-necked flask (500 mL) and dried under vacuum at 2 mmHg at 25 °C for 4 h. Dried THF (80 mL), followed by *n*-butyllithium (20 mmol), was added under nitrogen. The resulting solution was stirred at −30 °C for 30 min, during which 1-bromo-1′-lithioferrocene gradually precipitated. Acetaldehyde (20 mmol) or butyraldehyde (20 mmol) was then added, and the solution was stirred further at −30 °C for 30 min. Water (200 mL) was added, and the mixture was then extracted with CH_2Cl_2. The combined extracts were dried over $MgSO_4$ and evaporated at reduced pressure. The residue was chromatographed on Al_2O_3. The first band eluted with hexane was ferrocenes. Continued elution with hexane:CH_2Cl_2 (1:1) gave elutes which yielded the desired compound (89% yield for **18** and 86% yield for **19**). The physical properties are shown in Table 5.

Reduction of 18 and 19. The reduction reaction was carried out by carefully adding, with stirring, a small portion of $AlCl_3$ to a mixture of ferrocene compound and $LiAlH_4$ in dry ether. After 30 min, the solution became yellow, an excess of H_2O was added to it, and the ether layer was separated. The ether layer was washed with H_2O and dried over $MgSO_4$. After evaporation of the solvent, the crude product was chromatographed on Al_2O_3, eluting with hexane. The first band was the desired compound (∼95% yield). These compounds were identical by ^{1}H NMR with those prepared by a different procedure.[14,21]

General Ullman Coupling Reaction of 20−22 with 17. A mixture of the corresponding bromoferrocene (6.48 mmol), **17** (3.24 mmol), and activated Cu (10 g) was heated under N_2 at 125 °C (oil bath) for 24 h. The reaction mixture was cooled to room temperature and then subjected to the Soxhlet process with dichloromethane. The extract was evaporated at reduced pressure, and the residue was chromatographed on Al_2O_3.

Compound **23** was obtained by a cross-coupling reaction of **17** and **20**. The crude product was chromatographed, eluting with hexane. The first band was a mixture of ferrocene and ethylferrocene. The second band was 1′,1‴-diethylbiferrocene, which was identical by ^{1}H NMR with that prepared by a different procedure.[21] Continued elution with hexane:CH_2Cl_2 (20:1) gave the desired compound **23** (15% yield).

Compound **24** was obtained by a cross-coupling reaction of **17** and **21**. The purification was carried out by following the same procedure as described for **23**.

Compound **25** was obtained from **17** and **22**. The crude product was chromatographed, eluting with hexane. The first band was a mixture of ferrocenes. The second band eluted with hexane/ethyl acetate (50/1) was methoxymethylferrocene. Continued elution with hexane/ethyl acetate (100/7) gave 1′,1‴-dimethoxymethylbiferrocene (third band) and compound **25** (fourth band, 12.5% yield).

General Ullman Coupling Reaction of 20−22 with 26. The coupling reaction was carried out according to the general procedure described above, except using compound **26** instead of **17**.

Compound **27** was obtained by a cross-coupling reaction of **20** with **26**. The crude product was chromatographed, eluting with hexane. The first band was a mixture of ferrocenes. The second band was 1′,1‴-diethylbiferrocene, which was identical by ^{1}H NMR with that prepared by a different procedure.[21] Continued elution with hexane:benzene (1:1) gave the desired compound **27** (14% yield).

(20) Dong, T.-Y.; Lai, L. L. *J. Organomet. Chem.* **1996**, *509*, 131.

(21) Iijima, S.; Saida, R.; Motoyama, I.; Sano, H. *Bull. Chem. Soc. Jpn.* **1981**, *54*, 1375.

Compound **28** was obtained by a cross-coupling reaction of **21** with **26**. The crude product was chromatographed, eluting with hexane. The first band was a mixture of ferrocenes. Continued elution with hexane/CH_2Cl_2 (20/1) gave 1′,1‴-dibutylbiferrocene, which was identified by ^{1}H NMR.[14] Continued elution with hexane/CH_2Cl_2 (10/1) gave the desired compound **28** (9% yield).

Compound **29** was obtained by a cross-coupling reaction of **22** with **26**. The crude product was chromatographed, eluting with hexane. The first band was a mixture of biferrocenes. Continued elution with hexane/CH_2Cl_2 (10/1) gave 1′,1‴-dimethoxymethylbiferrocene.[5] Continued elution with hexane/CH_2Cl_2 (5/1) gave the desired compound **29** (9% yield).

Mixed-Valence Compounds 2−7. Samples of these mixed-valence compounds were prepared by adding a benzene/hexane (1:1) solution containing a stoichiometric amount of iodine to a solution of the corresponding polyferrocene at 0 °C. The corresponding polyferrocene solution was prepared by dissolving the polyferrocene in a proper solvent (benzene for **23**, **24**, and **27**−**29**; CH_2Cl_2 for **25**). The resulting dark crystals were filtered and washed repeatedly with cold hexane. Anal. Calcd for **2** ($C_{34}H_{34}Fe_3I_6$): C, 29.76; H, 2.50. Found: C, 28.94; H, 2.43. Anal. Calcd for **3** ($C_{38}H_{42}Fe_3I_6$): C, 31.97; H, 2.96. Found: C, 32.02; H, 2.79. Anal. Calcd for **4** ($C_{34}H_{34}Fe_3I_6O_2$): C, 29.09; H, 2.44. Found: C, 29.02; H, 2.39. Anal. Calcd for **5** ($C_{44}H_{42}Fe_4I_6$): C, 34.02; H, 2.86. Found: C, 33.97; H, 2.72. Anal. Calcd for **6** ($C_{48}H_{50}Fe_4I_6$): C, 35.77; H, 3.13. Found: C, 35.80; H, 3.13. Anal. Calcd for **7** ($C_{44}H_{42}Fe_4I_{11/2}$): C, 34.84; H, 2.75. Found: C, 34.67; H, 2.78.

Physical Methods. ^{57}Fe Mössbauer measurements were made on a constant-velocity instrument, which was previously described.[19] Velocity calibration was made using a 99.99% pure 10-μm iron foil. Typical line widths for all three pairs of iron foil lines fell in the range 0.24−0.27 mm s^{-1}. Isomer shifts are reported relative to iron foil at 300 K. Tabulated data is provided.

^{1}H NMR spectra were run on a Varian VXR-300 spectrometer. Mass spectra were obtained with a VG-BLOTECH-QUATTRO 5022 system.

Electrochemical measurements were carried out with a BAS 100W system. Cyclic voltammetry was performed with a stationary glassy carbon working electrode, which was cleaned after each run. These experiments were carried out with a 1 × 10^{-3} M solution of polyferrocene in dry CH_2Cl_2/CH_3CN (1:1) containing 0.1 M (n-$C_4H_9)_4NPF_6$ as the supporting electrolyte. The potentials quoted in this work are relative to a SCE electrode at 25 °C. Under these conditions, ferrocene shows a reversible one-electron oxidation wave ($E_{1/2}$ = 0.40 V).

The single-crystal X-ray determinations of all compounds were carried out on an Enraf-Nonius CAD4 diffractometer at 298 K. Absorption corrections were made with empirical ψ rotation. A three-dimensional Patterson synthesis was used to determine the heavy-atom positions, which phased the data sufficiently well to permit location of the remaining non-hydrogen atoms from Fourier synthesis. All non-hydrogen atoms were refined anisotropically. Hydrogen atoms were calculated at ideal distances. The X-ray crystal data are summarized in Table 1. Selected bond distances and angles are given in Tables 2, 3, and 5. Listings of the final positional parameters for all atoms, bond distances and angles, and thermal parameters of these compounds are given in the Supporting Information.

Structure Determination of 23. An orange crystal (0.19 × 0.44 × 0.50 mm) was obtained when a layer of hexane was allowed to slowly diffuse into a CH_2Cl_2 solution of **23**. Cell dimensions were obtained from 25 reflections with 14.38° < 2θ < 30.94°. The θ−2θ scan technique was used to record the intensities for all reflections for which 1° < 2θ < 49.8°. Of the 4593 unique reflections, there were 3201 reflections with $F_o > 2.0\sigma(F_o)$, where $\sigma(F_o)$ values were estimated from counting statistics.

Close examination of difference Fourier maps in the final stage of the structure solution revealed a disordered ethyl group in the Cp ring. The site occupancy factor of the ethyl substituent was set equal to 0.5.

Structure Determination of 25. An orange crystal (0.16 × 0.38 × 0.50 mm) was obtained following the same procedure as that described for **23**. Data were collected to a 2θ value of 55.0°. The unit cell dimensions were obtained from 25 reflections with 14.74° < 2θ < 34.20°. Of the 3109 unique reflections, there were 2472 with $F_o > 2.0\sigma(F_o)$.

Structure Determination of 29. An orange crystal (0.06 × 0.13 × 0.38 mm) was obtained following the same procedure as that described for **23**. The unit cell dimensions were obtained from 25 reflections with 11.78° < 2θ < 34.18°. Of the 3353 unique reflections, there were 2423 with $F_o > 2.0\sigma(F_o)$.

Close examination of difference Fourier maps in the final stage of the structure solution revealed a disordered methoxymethyl group in the Cp ring. The site occupancy factor of the methoxymethyl substituent was set equal to 0.5.

Acknowledgments are made to the National Science Council (Grant No. NSC87-2113-M-110-010), Taiwan, ROC, and Department of Chemistry at Sun Yat-Sen University.

Supporting Information Available: Complete tables of positional parameters, bond distances and angles, and thermal parameters for **23**, **25**, and **29** (19 pages). Ordering information is given on any current masthead page.

OM9801709